stellarator news

Published by Fusion Energy Division, Oak Ridge National Laboratory
Building 5700 P.O. Box 2008 Oak Ridge, TN 37831-6169, USA

Editor: James A. Rome Issue 111 October 2007
E-Mail: jar@ornl.gov Phone (865) 482-5643
On the Web at *http://www.ornl.gov/sci/fed/stelnews*

NCSX Review

A subcommittee of the U.S. Fusion Energy Sciences Advisory Committee (FESAC) reported conclusions of a science and program review of the National Compact Stellarator Experiment (NCSX) on October 23, 2007. The committee examined the scientific issues for compact stellarators, the role of NCSX in the international context, and the options for pursuing compact stellarator research. They concluded that NCSX would have a profound impact on stellarator research worldwide, noting that its compact quasi-axisymmetric design is unique in the world program.

The FESAC science review is one of a series of reviews conducted this year in response to NCSX construction cost and schedule issues. The NCSX vacuum vessel, 14 of the 18 modular coils (see Fig. 1), and 4 of the 18 toroidal field coils have been fabricated, and assembly activities have begun. In August, DOE's Office of Science reviewed a new plan for completing construction and preparing for the first plasma heating research campaign. The project presented a schedule with first plasma in 2012 and the first heating campaign in 2013. The review team found that completion of the project within the new cost and schedule estimates is achievable. An additional review, focusing on detailed engineering design and construction issues, is planned for early November. It is expected that the DOE will make decisions on the future of the NCSX project in the next few months.

More information about NCSX and slides for the upcoming construction review can be found at http://ncsx.pppl.gov/

G. H. Neilson
Princeton Plasma Physics Laboratory
Princeton, NJ 08543-0451 USA
E-mail: hneilson@pppl.gov

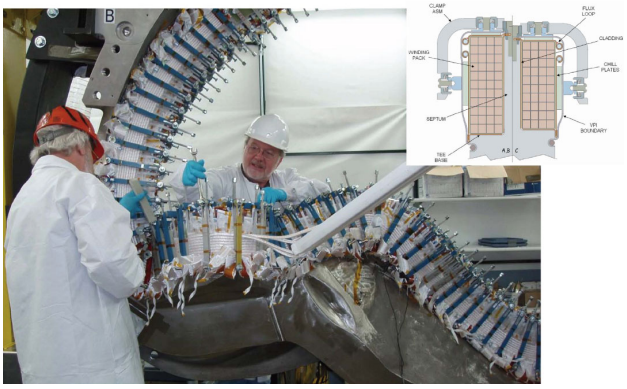

Fig. 1. Construction of the 14th modular NCSX coil is underway.

In this issue . . .

Theory of stellarators and tokamaks in three dimensions

The NSTAB computer code applies the MHD variational principle to calculate equilibrium and stability of toroidal plasmas in three dimensions. Differential equations are solved in a conservation form that describes force balance correctly across islands that are treated as discontinuities. The method has been applied to stellarators, including LHD, and tokamak configurations such as DIII-D and ITER. Despite the simplicity of the model, good correlation has been obtained with observations from experiments.

Sometimes the solution of the equations turns out not to be unique, and bifurcated equilibria that are nonlinearly stable may exist when theory predicts linear instability. The analysis shows that tokamak configurations such as ITER do not remain axially symmetric at finite beta, for they develop helical islands, which may manifest themselves experimentally as neoclassical tearing modes (NTMs) and edge-localized modes (ELMs). These results motivate a continuing search for improved stellarator configurations that employ relatively simple coils to generate good flux surfaces even at the low aspect ratios typical of a tokamak, retain the favorable high-beta equilibrium and stability characteristics of LHD, and promise reduced transport by virtue of quasiaxial symmetry (QAS).

The Maxwell stress tensor enables one to put the differential equations describing force balance in the conservation form

$$\nabla \cdot \left[\mathbf{BB} - \left(\frac{B^2}{2} + p \right) \mathbf{I} \right] = 0, \nabla \cdot \mathbf{B} = 0 .$$

Comparable finite difference equations, summed over a test volume, telescope down to a correct statement of force balance over the boundary. In this way we capture discontinuities in Clebsch solutions

$$\mathbf{B} = \nabla s \times \nabla \theta = \nabla \phi + \zeta \nabla s$$

of the MHD variational principle

$$\delta \iiint \left(\frac{B^2}{2} - p(s) \right) dV = 0$$

for a plasma with separatrix defined by the Fourier series

$$r + iz = \mathrm{e}^{iu} \sum \Delta_{mn} \mathrm{e}^{-imu + inv} .$$

Islands occur where the spectrum B_{mn}, defined by

$$\frac{1}{B^2} = \sum B_{mn}(s) \cos[m\theta - (n - \iota m)\phi]) ,$$

activates small denominators of the parallel current,

$$\frac{\mathbf{J} \cdot \mathbf{B}}{p' B^2} = \sum \frac{m B_{mn}(s)}{n - \iota m} \cos[m\theta - (n - \iota m)\phi] .$$

An example of a discontinuous solution occurs in the RFP model problem

$$(\Psi_x{}^2)_x = \eta \Psi_{xxx}, \quad \Psi = 1 - |x| .$$

These equations have been implemented in the NSTAB computer code. The accompanying figures demonstrate code results for LHD and ITER.

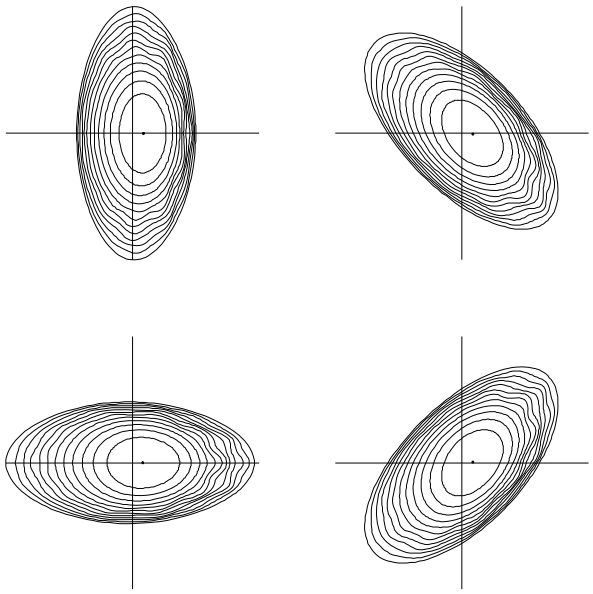

Fig. 1. Poincaré sections of the flux surfaces of a bifurcated, nonlinearly stable LHD equilibrium at $\beta = 0.048$. The ripple in the flux surfaces on the right suggests that ballooning modes appear in the solution, but a reliable prediction of the limit cannot be made without more information about the experiment. The existence of several solutions of the ideal MHD equilibrium equations is considered to be evidence of linear instability.

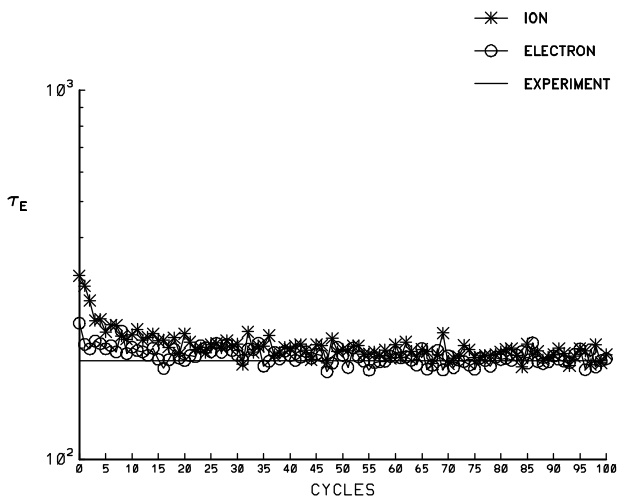

Fig. 2. Cycles of a calculation of the energy confinement time τ_E in milliseconds for a neutral beam injection (NBI) shot of the LHD experiment using a quasineutrality algorithm to adjust the electric potential Φ. Oscillations of Φ along the magnetic lines produce realistic transport, so there is good agreement with the observed value. Results from the LHD experiment have served to validate the numerical simulations of equilibrium, stability, and transport that are provided by runs of the NSTAB and TRAN computer codes. The TRAN code models thermal transport by performing a random walk among complicated orbits of the ions or electrons, which are found from Runge-Kutta solutions of a system of ordinary differential equations for guiding centers. The results depend primarily on the magnetic spectrum of the plasma, which is obtained from runs of the NSTAB code.

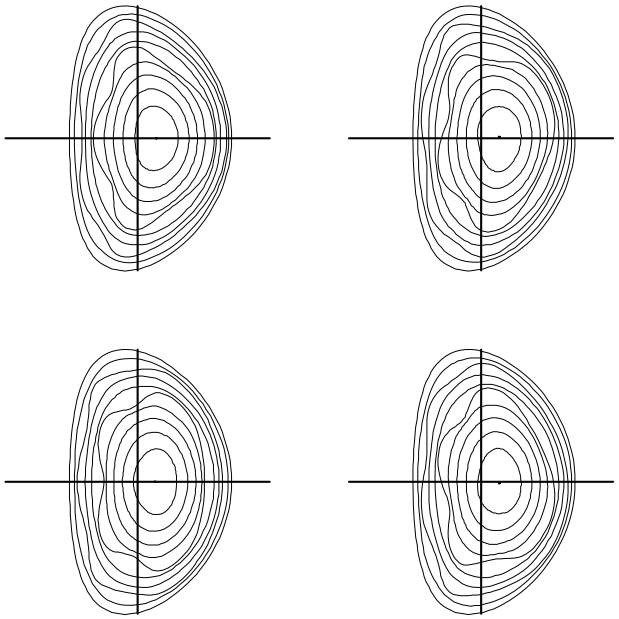

Fig. 3. Four Poincaré sections of the magnetic surfaces over one of three artificial field periods of a bifurcated, nonlinearly stable ITER equilibrium at $\beta = 0.03$ with $0.9 > \iota > 0.4$. The ripple in the flux surfaces suggests that there may be NTMs and ELMs in this three-dimensional solution of an axially symmetric problem. Extensive studies of numerical examples produce ample evidence that bifurcated equilibria can be expected to appear in most tokamak problems, so provision should be made for that. Convergent runs of the NSTAB code can capture islands whose widths are smaller than the radial mesh size and compute bifurcated equilibria in examples where there is marginal linear instability, but global nonlinear stability, of the ideal MHD model.

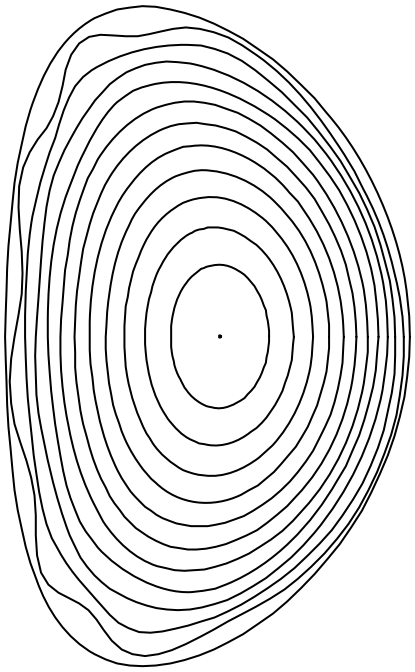

Fig. 4. Poincaré section of the flux surfaces of a bifurcated ITER equilibrium at $\beta = 0.027$ with net current bringing the rotational transform into the interval $0.93 > \iota > 0.37$. There are helical islands in this three-dimensional solution of an axially symmetric MHD problem, which may model ELMs. A forcing term was used early in the run to trigger a mode that appears as a discontinuity in the three-dimensional solution. This double-precision calculation converges to the level of round-off error, showing that the discrete problem has been solved. Islands are captured numerically by finite difference equations in a conservation form that works despite the nested surface hypothesis present in our mathematical formulation of the problem. The results are plausible on the long time scale of a magnetic fusion reactor.

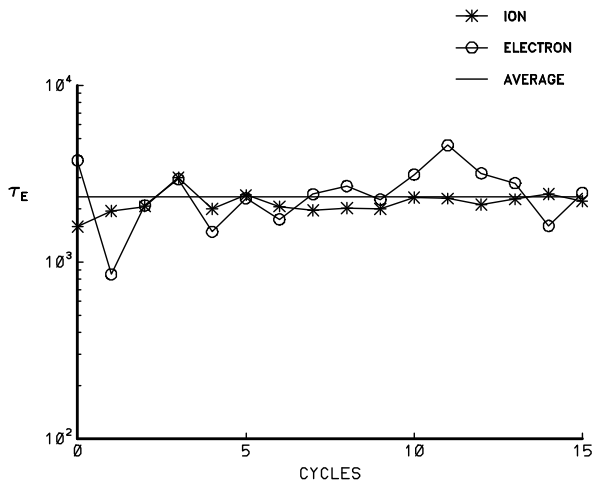

Fig. 5. Cycles of a calculation of the energy confinement time τ_E (in milliseconds) for the ITER tokamak using a quasineutrality algorithm to adjust the electric potential Φ. The three-dimensional effect of ripple associated with a system of only 12 toroidal coils has been introduced to drive the radial electric field and cause the plasma to spin. It is not clear that two-dimensional models adequately describe transport in tokamaks. The energy confinement time is calculated from an empirical relationship with the particle confinement time. Without three-dimensional terms we have not been able to reconcile discrepancies between the ion and electron confinement times that are computed by the Monte Carlo method in tokamaks.

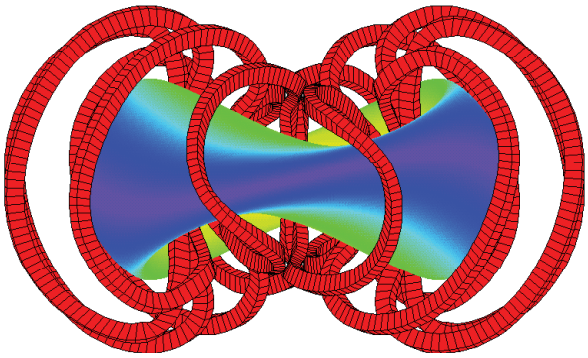

Fig. 6. Diagram of a compact stellarator with two field periods. The color map of the plasma displays a QAS of the magnetic spectrum that enhances confinement. The 12 moderately twisted coils generate a magnetic field designed to keep the plasma in stable equilibrium separated from material walls. The side view of this optimized configuration shows that there is ample space between the coils for NBI heating. A judiciously optimized QAS stellarator may overcome poor transport and low ion temperature observed in conventional stellarators, and with the poor stability and ELM crashes observed in tokamaks.

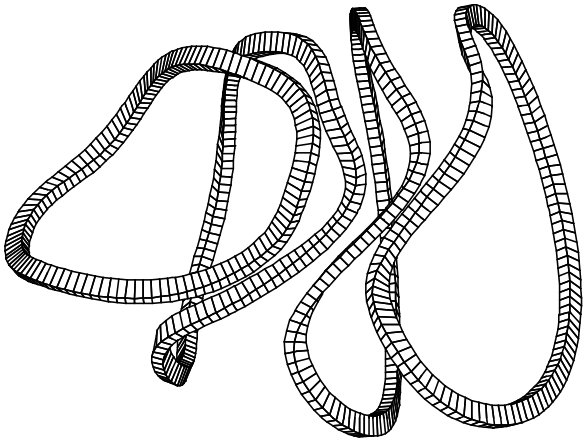

Fig. 7. Four out of 12 modular coils of the MHH2 stellarator in a vacuum magnetic field defined by elementary potential theory. The coils at the sides of the diagram are located at corners over the full torus, so the distances between all the coils can be estimated from the figure. Judicious filtering of the Fourier series used to calculate filaments specifying the geometry of the configuration defines shapes that are not excessively twisted. Parameters have been adjusted to provide ample space around each coil, and the aspect ratio of the plasma is 2.5. The spacing is adequate for superconducting coils in a reactor with a major radius of 7 m or 8 m, but there is difficulty fitting the coils together inside a small experiment at high magnetic field. Through rigid motions, four copies of the quadrant of coils shown in the plot can be combined to give an accurate picture over the full torus.

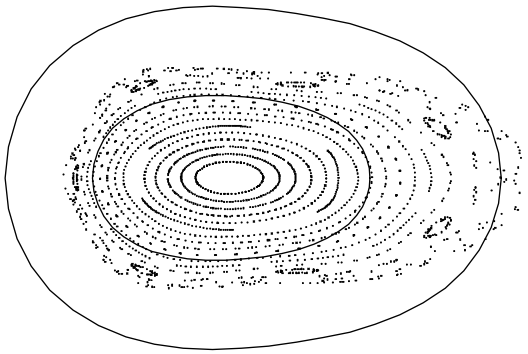

Fig. 8. Cross section of a line tracing calculation for a QAS stellarator displaying curves that define the control surface for the coils and the shape of the plasma, together with magnetic lines computed at $\beta = 0$. The flux surfaces and islands outside the separatrix show that the magnetic field is well organized for a divertor. This works because smooth coils were found to provide the external field confining the plasma. It is essential to choose the coils both so that the stellarator can be constructed without too much difficulty and so that the flux surfaces remain robust when realistic changes are made in physical parameters. The formulas that we apply to represent the plasma surface and the shape of the coils are motivated by a knowledge of interpolation and approximation in the theory of analytic functions of a complex variable.

References

[1] R. Alexander and P. Garabedian, Choice of coils for a fusion reactor, Proc. Natl. Acad. Sci. USA **104** (2007) 12250–12252.

[2] P. Garabedian and M. Taylor, Tokamak transport driven by quasineutrality and helical asymmetry, Nucl. Fusion **32** (1992) 265–270.

[3] S. Hirshman and O. Betancourt, Preconditioned descent algorithm for rapid calculations of magnetohydrodynamic equilibria, J. Comput. Phys. **96** (1991) 99–109.

[4] M. Taylor, A high performance spectral code for nonlinear MHD stability, J. Comput. Phys. 110 (1994) 407–418.

Paul R. Garabedian
Courant Institute, New York University
251 Mercer Street
New York, N.Y. 10012-1185
E-mail: garabedi@cims.nyu.edu

Observation of an impurity hole structure in LHD

It is desirable to minimize impurities in the core of a hot fusion plasma because impurities cause reduction of the fusion power density by enhancing the cooling of the plasma by radiation and also by diluting the hydrogen fuel. Therefore, impurity profiles have been observed with keen interest because the transport and behavior of impurities strongly affect the characteristics of the plasma in magnetically confined fusion experiments. Here, we report that an extreme hollow profile of the impurity carbon has been observed in a high-ion-temperature plasma in the Large Helical Device (LHD) in Toki, Japan.

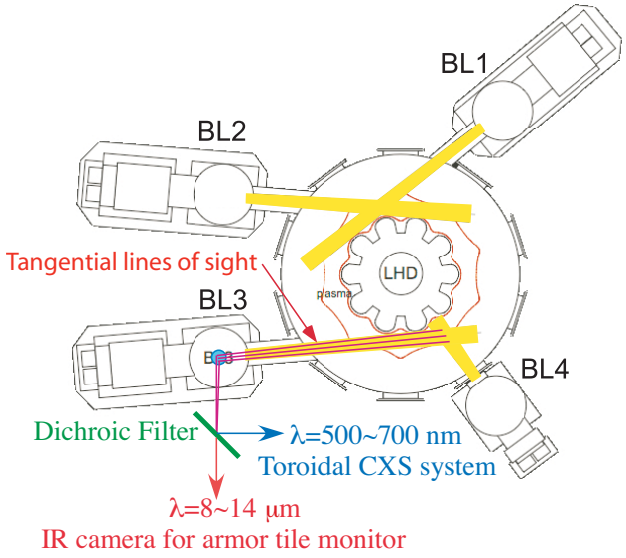

Fig. 1. Tangential lines of sight for charge-exchange spectroscopy on LHD.

Recently, a tangential line-of-sight charge-exchange spectrometer (CXS) was installed on LHD as shown in Fig. 1. Emission from charge exchange of carbon with a 40-keV neutral beam (BL4) are led to the fiber bundle by optics installed in the view port for the armor tile monitor at BL3. A dichroic filter is used to separate the light into a visible component for the CXS and an infrared (IR) component for the IR camera. The tangential line of sight has the advantage that the line-integrated signal of charge-exchange emission is less affected by the impurity profiles, while the noncentral charge-exchange emission is dominant on the line-integrated signal using a poloidal line of sight when the impurity profile becomes extremely hollow. An impurity hole is clearly observed in a discharge with injection of a single carbon pellet, which is intended to increase the deposition of the high-energy neutral beam (~160 keV) and to increase the ion temperature. The magnetic field strength $B_0 = -2.676$ T, the position of magnetic axis $R_{ax} = 3.6$ m, the pitch parameter $\gamma = 1.254$, and the canceling rate of the quadrupole field $B_q = 100\%$.

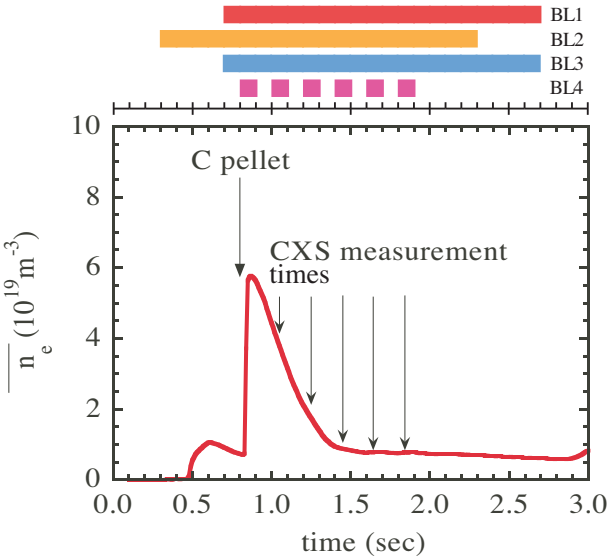

Fig. 2. Line-averaged electron density measured with FIR interferometer. The bars at the top indicate the durations of neutral beam injection from each beamline.

Figure 2 shows the time evolution of the line-averaged electron density measured with the far infrared (FIR) interferometer. Neutral beam injection times are indicated by the bars at the top in Fig. 2, and the carbon pellet injection times and the CXS measurement times are indicated with the arrows. The electron density rapidly increases just after the injection of the carbon pellet at 0.8 s and then decreases on a time scale of a few hundred ms, while the plasma is sustained with three tangentially injected negative ion source neutral beams (BL1, BL2, BL3), and a modulated neutral beam which has a positive ion source (BL4). BL4 has been modulated to be on for 100 ms and off for 100 ms to provide the both the signal and the background for CXS. The ion temperature increases during the decay phase of the electron density. Figure 3 shows the profiles of the ion temperature and the toroidal rotation velocity. The ion temperature profile changes during the decay phase of the electron density. The ion temperature gradient after $t = 1.45$ s becomes more steep around $R = 4.1$ m, and becomes more gradual outside $R = 4.3$ m compared with the ion temperature profile at $t = 1.25$ s. This suggests that there is an improvement of ion transport inside the plasma. It is also observed that the strong toroidal rotation is driven in the co-direction by the neutral beams associated with the increase of the ion temperature.

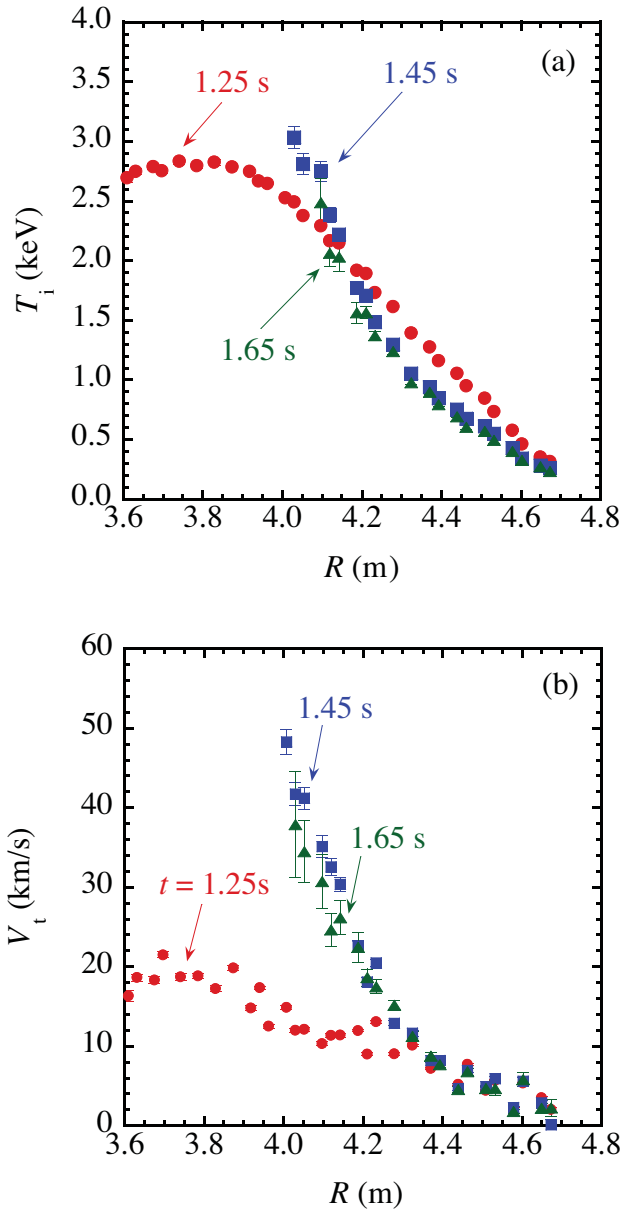

Fig. 3. Profiles of (a) ion temperature and (b) toroidal rotation velocity at t = 1.25 s (circles), 1.45 s (squares), and 1.65 s (triangles).

Figure 4 shows the time evolution of the density of the carbon impurity at different radial positions. Decay times of the carbon impurity in the inner region (R = 3.9 m, 4.1 m) are much shorter than in the outer region (R = 4.5 m, 4.6 m). The profile becomes perfectly hollow at t = 1.65 s, while it is peaked at t = 1.25 s. Figure 5 shows profiles of carbon density and electron density. Both are observed to be peaked at t = 1.25 s. The profile of the carbon impurity is observed to be extremely hollow, while the electron density is observed to be peaked or almost flat at t = 1.65 s. This suggests that a strong outward flow of impurities may sustain the hollow profiles. The ratio of carbon density to ion density reached 0.3% at the plasma center, and 10% near the edge (R = 4.4 m).

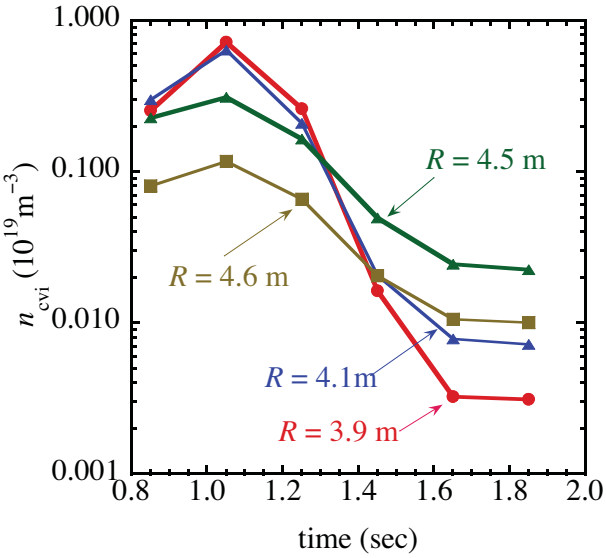

Fig. 4. Time evolution of carbon impurity density at R = 3.9 m (circles), R = 4.1 m (squares), R = 4.5 m (triangles), and R = 4.6 m (diamonds).

In summary, carbon impurity profiles have been measured with CXS using the charge-exchange line of fully ionized carbon with a toroidal line of sight. The impurity profile becomes extremely hollow, while the ion temperature increases during the decay phase of the electron density in this experiment. The ratio of carbon density to ion density was 0.3% at the plasma center with the impurity hole. The impurity hole is considered to be beneficial for the fusion plasma.

Mikirou Yoshinuma
National Institute for Fusion Science
Toki, Japan
E-mail: yoshinuma@nifs.ac.jp

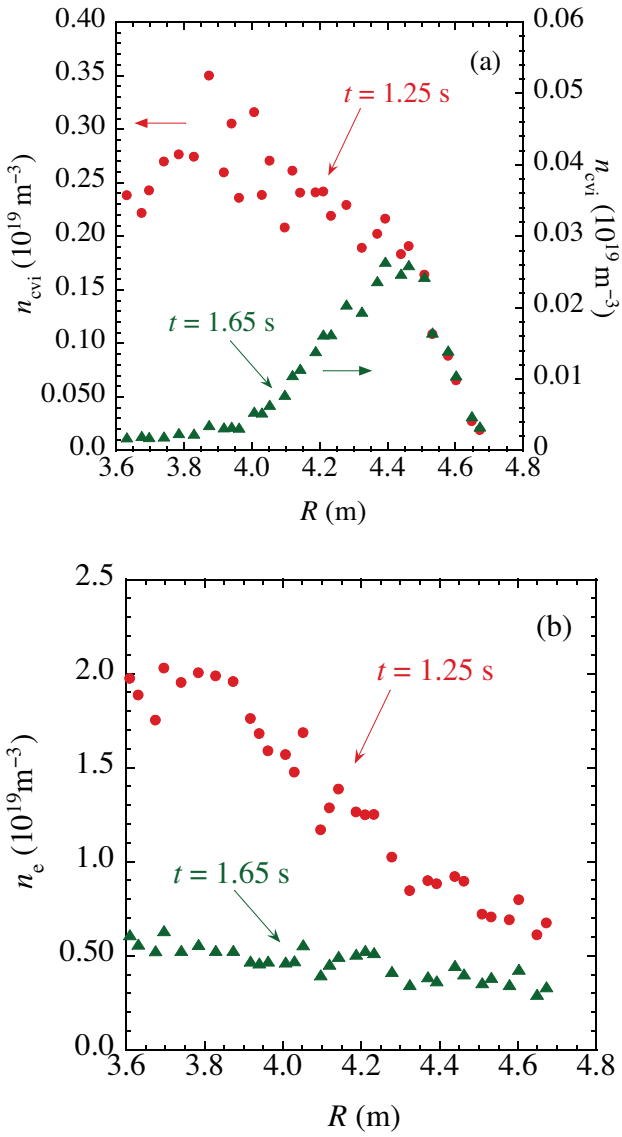

Fig. 5. Profiles of (a) carbon density and (b) electron density at $t = 1.25$ s (circles) and $t = 1.65$ s (triangles).